Pergamon

J. Quant. Spectrosc. Radiat. Transfer Vol. 51, No. 3, pp. 491–510, 1994
Elsevier Science Ltd. Printed in Great Britain
0022-4073(94)E0012-U 0022-4073/94 $7.00 + 0.00

ERRORS INDUCED BY THE NEGLECT OF POLARIZATION IN RADIANCE CALCULATIONS FOR RAYLEIGH-SCATTERING ATMOSPHERES

M. I. MISHCHENKO,†‡ A. A. LACIS,§ and L. D. TRAVIS§

†NASA Goddard Institute for Space Studies/Hughes STX Corporation, 2880 Broadway, New York, NY 10025 and §NASA Goddard Institute for Space Studies, 2880 Broadway, New York, NY 10025, U.S.A.

(Received 6 May 1993)

Abstract—Although neglecting polarization and replacing the rigorous vector radiative transfer equation by its approximate scalar counterpart has no physical background, it is a widely used simplification when the incident light is unpolarized and only the intensity of the reflected light is to be computed. In this paper we employ accurate vector and scalar multiple-scattering calculations to perform a systematic study of the errors induced by the neglect of polarization in radiance calculations for a homogeneous, plane-parallel Rayleigh-scattering atmosphere (with and without depolarization) above a Lambertian surface. Specifically, we calculate percent errors in the reflected intensity for various directions of light incidence and reflection, optical thicknesses of the atmosphere, single-scattering albedos, depolarization factors, and surface albedos. The numerical data displayed can be used to decide whether or not the scalar approximation may be employed depending on the parameters of the problem. We show that the errors decrease with increasing depolarization factor and/or increasing surface albedo. For conservative or nearly conservative scattering and small surface albedos, the errors are maximum at optical thicknesses of about 1. The calculated errors may be too large for some practical applications, and, therefore, rigorous vector calculations should be employed whenever possible. However, if approximate scalar calculations are used, we recommend to avoid geometries involving phase angles equal or close to 0° and 90°, where the errors are especially significant. We propose a theoretical explanation of the large vector/scalar differences in the case of Rayleigh scattering. According to this explanation, the differences are caused by the particular structure of the Rayleigh scattering matrix and come from lower-order (except first-order) light scattering paths involving right scattering angles and right-angle rotations of the scattering plane.

1. INTRODUCTION

Although neglecting the vector nature of light and replacing the rigorous vector radiative transfer equation by its approximate scalar counterpart has no physical background, it is a widely used simplification when the incident light is unpolarized and only the intensity of multiply scattered light is to be computed. The errors in the reflected intensity resulting from the neglect of polarization were examined by Hansen[1] on the basis of accurate adding/doubling calculations of multiple scattering. He concluded that in most cases the errors in the scalar approximation should be less than or of the order of 1% for light reflected by a cloud of spherical particles with sizes of the order of or larger than the wavelength of light, which makes the scalar approximation applicable in radiance calculations for cloud and aerosol layers. On the other hand, it has been known since the pioneering work by Chandrasekhar[2] that the errors can be much larger in the case of a semi-infinite atmosphere with pure Rayleigh scattering. For light reflected by finite Rayleigh atmospheres Adams and Kattawar[3] found errors up to 11.7%. Similar large errors are seen in Table 43 of van de Hulst.[4] However, although the problem of multiple Rayleigh scattering in both vector and scalar formulations was studied, for example, in Refs. 2–8 and references therein, in great detail, no systematic study of the large errors induced by neglecting polarization was performed

‡To whom all correspondence should be addressed.

and no theoretical explanation of the errrors was suggested. On the other hand, such an investigation would be of importance for terrestrial and planetary remote sensing studies.[9–14] Therefore, it is the aim of the present paper to fill out this gap. Specifically, on the basis of accurate vector and scalar calculations of multiple light scattering, we systematically examine the vector/scalar differences in the intensity of the radiation reflected by a homogeneous Rayleigh-scattering atmosphere for various directions of light incidence and reflection, single scattering albedos, depolarization factors, optical thicknesses of the atmosphere, and albedos of the underlying surface, and discuss the corresponding implications for remote sensing studies.

2. BASIC DEFINITIONS

To describe the state of polarization of a beam of light we use the Stokes parameters I, Q, U, and V as defined for example by Hansen and Travis.[15] The Stokes vector $\mathbf{I}$ is defined as a (4×1) column matrix of Stokes parameters as follows:

$$\mathbf{I} = \{I, Q, U, V\} = \begin{bmatrix} I \\ Q \\ U \\ V \end{bmatrix}. \tag{1}$$

To specify the direction of light propagation in a plane-parallel atmosphere we use the couple (u, ϕ), where $u = \cos \vartheta$, ϑ is the angle between this direction and the inward normal to the upper boundary to the slab, and ϕ is the azimuth angle which is measured clockwise when looking upwards. Also, we define $\mu = |u|$. The upper boundary of the atmosphere is illuminated by an unpolarized beam of light incident in the direction $(\mu_0, \phi_0 = 0)$ and specified by the flux vector $\pi \mathbf{F}_{\text{inc}} = \pi\{1, 0, 0, 0\}$. Multiple light scattering in a homogeneous, plane-parallel, macroscopically isotropic atmosphere is described by the (vector) radiative transfer equation[15,16]

$$u \frac{\mathrm{d}\mathbf{I}(\tau, u, \phi)}{\mathrm{d}\tau} = -\mathbf{I}(\tau, u, \phi) + \frac{\bar{\omega}}{4\pi} \int_0^{2\pi} \mathrm{d}\phi' \int_{-1}^{1} \mathrm{d}u' \bar{Z}(u, \phi, u', \phi') \mathbf{I}(\tau, u', \phi') + \frac{\bar{\omega}}{4} \bar{Z}(u, \phi, \mu_0, 0) \mathbf{F}_{\text{inc}} \exp(-\tau/\mu_0) \tag{2}$$

subject to standard boundary conditions

$$\begin{cases} \mathbf{I}(0, u, \phi) = 0, \quad u > 0, \\ \mathbf{I}(\tau_0, u, \phi) = \dfrac{1}{\pi} \displaystyle\int_0^{2\pi} \mathrm{d}\phi' \int_0^1 \mathrm{d}\mu' \bar{R}_{\text{surf}}(u, \phi, \mu', \phi') \mathbf{I}(\tau_0, \mu', \phi') \mu' \\ \qquad + u_0 \bar{R}_{\text{surf}}(u, \phi, \mu_0, \phi_0) \mathbf{F}_{\text{inc}} \exp(-\tau_0/\mu_0), \quad u < 0. \end{cases} \tag{3}$$

Here, τ_0 is the optical thickness of the atmosphere, τ is the optical depth, $\tilde{\omega}$ is the albedo for single scattering, $\bar{Z}$ is the (4×4) single-scattering phase matrix, and $\bar{R}_{\text{surf}}$ is the (4×4) reflection matrix of the underlying surface. The phase matrix describes the single-scattering transformation of the Stokes vector of the incident light into the Stokes vector of the scattered light provided that both Stokes vectors are specified with respect to the corresponding local meridional planes [i.e., the planes through the light beams and the local normal $(u = 1)$]. Usually, the single-scattering transformation law is defined with respect to the scattering plane (i.e., the plane through the incident and scattered beams) by means of the (4×4) scattering matrix $\bar{P}(\Theta)$, where Θ is the scattering angle. In this case

$$\bar{Z}(u', \phi', u, \phi) = \bar{L}(i_2) \bar{P}(\Theta) \bar{L}(i_1), \tag{4}$$

where the angles i_1 and i_2 are shown in Fig. 1, and

$$\bar{L}(\beta) = \begin{bmatrix} 1 & 0 & 0 & 0 \\ 0 & \cos 2\beta & \sin 2\beta & 0 \\ 0 & -\sin 2\beta & \cos 2\beta & 0 \\ 0 & 0 & 0 & 1 \end{bmatrix} \tag{5}$$

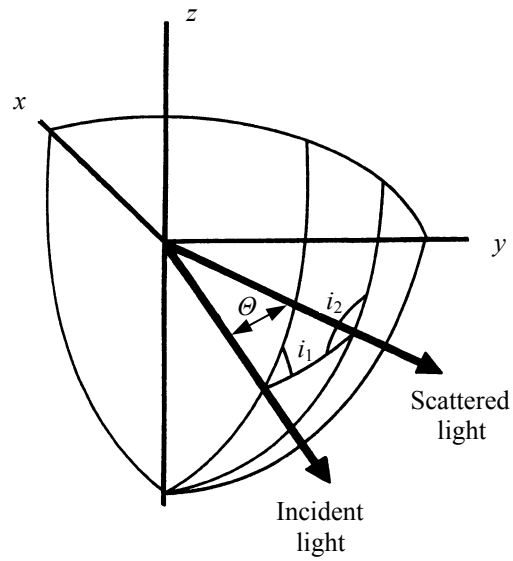

Fig. 1. On the definition of the phase matrix.

is the rotation matrix which describes the transformation of the Stokes vector when the reference plane is rotated around the light beam at an angle β measured anti-clockwise when looking in the direction of light propagation.

For a purely gaseous atmosphere consisting of randomly oriented anisotropic molecules, the scattering matrix has the form[15]

$$\bar{P}(\Theta) = \Delta \begin{bmatrix} \frac{3}{4}(1+\cos^2\Theta) & -\frac{3}{4}\sin^2\Theta & 0 & 0 \\ -\frac{3}{4}\sin^2\Theta & \frac{3}{4}(1+\cos^2\Theta) & 0 & 0 \\ 0 & 0 & \frac{3}{2}\cos\Theta & 0 \\ 0 & 0 & 0 & \Delta'\frac{3}{2}\cos\Theta \end{bmatrix} + (1-\Delta) \begin{bmatrix} 1 & 0 & 0 & 0 \\ 0 & 0 & 0 & 0 \\ 0 & 0 & 0 & 0 \\ 0 & 0 & 0 & 0 \end{bmatrix}, \tag{6}$$

where

$$\Delta = \frac{1-\delta}{1+\delta/2}, \tag{7}$$

$$\Delta' = \frac{1-2\delta}{1-\delta}, \tag{8}$$

and δ is the depolarization factor. For pure Rayleigh scattering, the depolarization factor vanishes, while for most gases it substantially deviates from zero. For example, δ is close to 0.03 for air and 0.09 for CO_2.

In the scalar approximation, the Stokes vector $\mathbf{I}$ is replaced by its first element I (i.e., intensity), and all the (4×4) matrices are replaced by their (1,1)-elements. Throughout the paper, we will supply rigorously calculated "vector" quantities by the superscript "v", while approximate "scalar" quantities will be supplied by the superscript "s". To describe the errors in the reflected intensity resulting from the use of the scalar approximation, we will use several definitions. The percent error $\epsilon(\tau_0, \mu, \mu_0, \phi)$ is defined as

$$\epsilon(\tau_0, \mu, \mu_0, \phi) = \frac{I^{\mathrm{v}}(0, -\mu, \phi) - I^{\mathrm{s}}(0, -\mu, \phi)}{I^{\mathrm{v}}(0, -\mu, \phi)} \times 100\%, \quad \mu_0 \in [0, 1], \quad \mu \in [0, 1], \quad \phi \in [0, 2\pi]. \tag{9}$$

The degree to which the scalar approximation underestimates the intensity for given τ_0, μ, and μ_0 is specified by the local underestimation $\epsilon_u(\tau_0, \mu, \mu_0)$ defined by

$$\epsilon_u(\tau_0, \mu, \mu_0) = \max_{\phi \in [0, 2\pi]} \epsilon(\tau_0, \mu, \mu_0, \phi). \tag{10}$$

Note that for some particular values of μ and μ_0, the local underestimation may be negative thus implying that the scalar approximation overestimates the intensity for all $\phi \in [0, 2\pi]$. Analogously, the local overestimation $\epsilon_0(\tau_0, \mu, \mu_0)$ is defined by

$$\epsilon_o(\tau_0, \mu, \mu_0) = \min_{\phi \in [0,2\pi]} \epsilon(\tau_0, \mu, \mu_0, \phi), \tag{11}$$

and a positive local overestimation for some μ and μ_0 means that the scalar approximation underestimates the intensity for all $\phi \in [0, 2\pi]$. Correspondingly, the maximum underestimation $\epsilon_u^{max}(\tau_0)$ is given by

$$\epsilon_u^{max}(\tau_0) = \max_{\mu \in [0,1], \mu_0 \in [0,1]} \epsilon_u(\tau_0, \mu, \mu_0), \tag{12}$$

while the maximum overestimation is defined as

$$\epsilon_o^{max}(\tau_0) = -\min_{\mu \in [0,1], \mu_0 = [0,1]} \epsilon_o(\tau_0, \mu, \mu_0). \tag{13}$$

The azimuthal angles at which the local underestimation and local overestimation are reached are denoted by $\phi_u(\tau_0, \mu, \mu_0)$ and $\phi_o(\tau_0, \mu, \mu_0)$, respectively, while the corresponding phase angles are denoted by $\alpha_u(\tau_0, \mu, \mu_0)$ and $\alpha_o(\tau_0, \mu, \mu_0)$. [The phase angle α is the angle between the direction of light reflection given by $(-\mu, \phi)$ and the direction opposite to the direction of light incidence and given by $(-\mu_0, \pi)$.]

A quantity widely used in planetary astrophysics is the geometric albedo $A_g(\tau_0)$ given by[17]

$$A_g(\tau_0) = 2\int_0^1 d\mu_0 I(0, -\mu_0, \pi)\mu_0. \tag{14}$$

The percent error in A_g resulting from the use of the scalar approximation is defined by

$$\epsilon_A(\tau_0) = \frac{A_g^v(\tau_0) - A_g^s(\tau_0)}{A_g^v(\tau_0)} \times 100\%. \tag{15}$$

In both vector and scalar calculations of light reflection by finite atmospheres, we use the adding/doubling method, as described in Refs. 1, 4, 15, and 18, and the invariant imbedding approach, as developed in Refs. 19 and 20. Extensive accuracy tests have shown excellent agreement between these two numerical techniques. For simplicity, we assume that the underlying surface is Lambertian with albedo A_L, i.e. the surface reflection matrix has the form

$$\bar{R}_{surf} = \begin{bmatrix} A_L & 0 & 0 & 0 \\ 0 & 0 & 0 & 0 \\ 0 & 0 & 0 & 0 \\ 0 & 0 & 0 & 0 \end{bmatrix}. \tag{16}$$

In computations for semi-infinite atmospheres, we employ an iterative solution of Ambartsumian's nonlinear integral equation for the reflection matrix (function), as suggested in Refs. 21 and 22.

3. CALCULATIONS AND DISCUSSION

In order to keep the paper to a reasonable size, we display here only the most representative computations which illustrate our basic conclusions. In Figs. 2–7 we show the maximum underestimation $\epsilon_u^{max}(\tau_0)$ and maximum overestimation $\epsilon_o^{max}(\tau_0)$ and the error in the geometric albedo $\epsilon_A(\tau_0)$ for different single scattering albedos $\tilde{\omega}$, depolarization factors δ, and Lambertian albedos A_L. These plots can be used in practice to decide whether the scalar approximation may be used or rigorous vector calculations should be employed. One sees that the vector/scalar

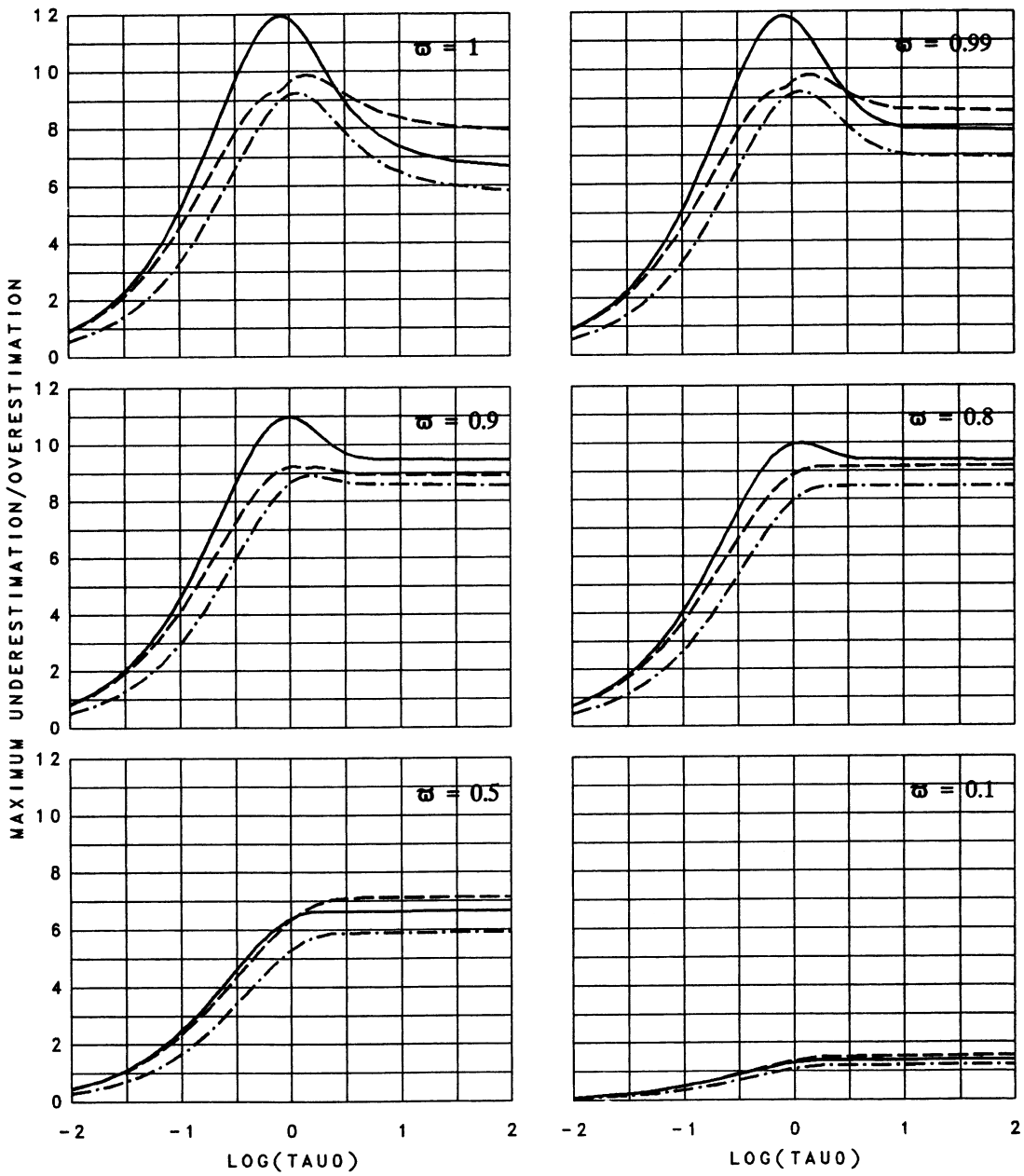

Fig. 2. Maximum overestimation $\epsilon_o^{max}(\tau_0)$ (solid lines) and maximum underestimation $\epsilon_u^{max}(\tau_0)$ (dashed lines) and the error in the geometric albedo $\epsilon_A(\tau_0)$ (dot–dashed lines) for $\delta = 0$, $A_L = 0$, and single scattering albedos $\tilde{\omega} = 1$, 0.99, 0.9, 0.8, 0.5, and 0.1.

differences decrease with increasing depolarization factor and/or increasing surface albedo. For optically thin layers ($\tau_0 < 1$), vector/scalar differences always decrease with decreasing single-scattering albedo. In the limit $\tau_0 \to 0$, Eq. (9) can be rewritten in terms of contributions of the first and second orders of scattering to the reflected intensity (supplied by subscripts 1 and 2, respectively) as

$$\epsilon \approx \frac{\tilde{\omega}(I_2^v - I_2^s)}{I_1^v + \tilde{\omega} I_2^v} \times 100\%, \tag{17}$$

which explains the $\tilde{\omega}$-dependence for $\tau_0 < 1$.[23] [In Eq. (17) we have taken into account that for unpolarized incident light $I_1^v = I_1^s$]. For optically thick atmospheres ($\tau_0 \gg 1$), vector/scalar differ-

ences first increase as the single-scattering albedo decreases from 1 to about 0.8, but then decrease with further decrease of $\tilde{\omega}$. With $\tau_0 \to \infty$, all the curves tend to the corresponding asymptotic limits which are independent of the surface albedo and depend only on the albedo for single scattering $\tilde{\omega}$ and depolarization factor δ. For single scattering albedos equal or close to unity (conservative or nearly conservative scattering) and small surface albedos, the curves have a characteristic maximum near $\tau_0 \approx 1$ which disappears with increasing absorption and/or increasing surface albedo. All three errors displayed in Figs. 2–7 have roughly the same order of magnitude.

Figures 8–16 illustrate the angular distribution of vector/scalar differences for $\tau_0 = 1$, $\tilde{\omega} = 1$, $\delta = 0.031$, and $A_L = 0$. Note, however, that the contour plots displayed are rather typical and, in conjunction with Figs. 2–7, give a general idea of what can be expected for other values of the optical thickness, albedo for single scattering, depolarization factor, and surface albedo. Moreover,

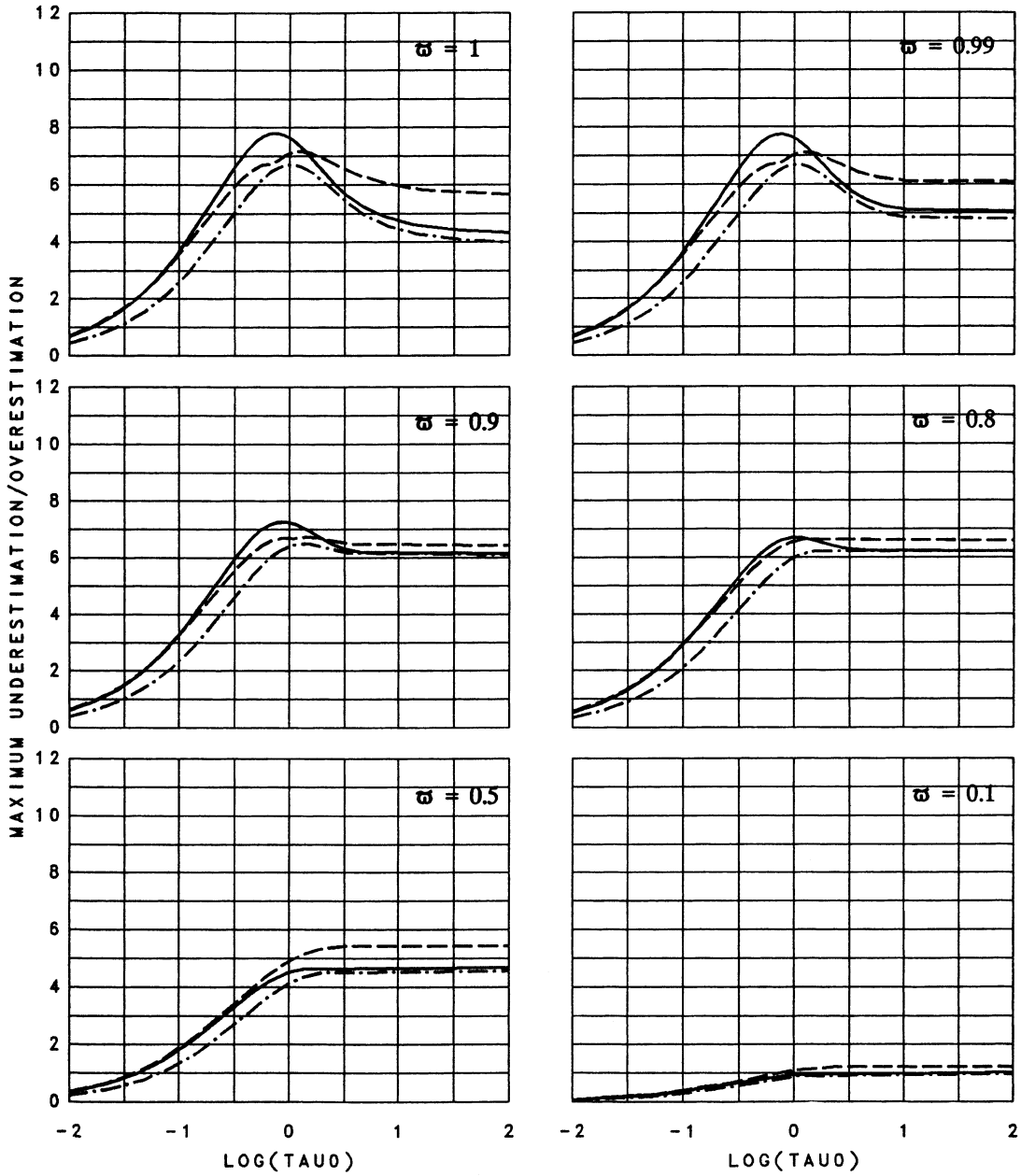

Fig. 3. Same as in Fig. 2, but for $\delta = 0.086$.

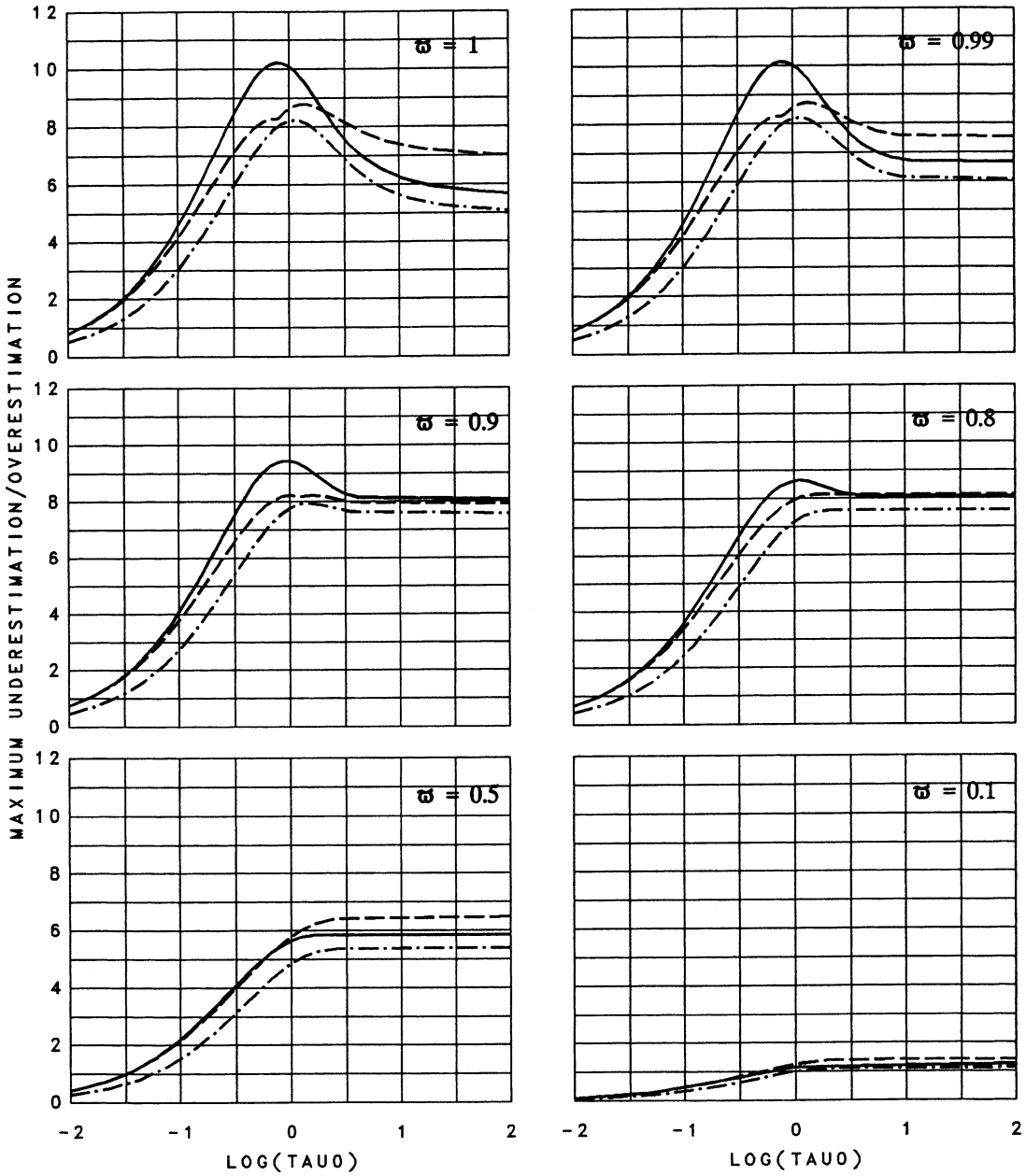

Fig. 4. Same as in Fig. 2, but for $\delta = 0.031$.

we have found that, independently of the parameter values, the local underestimation is always reached in the azimuth plane $\phi = 180°$, i.e.

$$\phi_u(\tau_0, \mu, \mu_0) \equiv 180°. \tag{18}$$

[Note that the step size in azimuth angle in our calculations of $\phi_u(\tau_0, \mu, \mu_0)$ was only 0.2°, thus making the identity (18) numerically very accurate.] Therefore, the contour plot of $\alpha_u(\tau_0, \mu, \mu_0)$ shown in Fig. 14 is exactly the same for any τ_0, $\tilde{\omega}$, δ, and A_L. Also, owing to the identity of Eq. (18), the contour plot of the percent error $\epsilon(\tau_0, \mu, \mu_0, 180°)$ shown in Fig. 12 is at the same time the contour plot of the local underestimation $\epsilon_u(\tau_0, \mu, \mu_0)$. Owing to reciprocity, Figs. 8–16 are symmetrical with respect to the diagonal $\mu = \mu_0$.

One sees from Figs. 8–12 that the vector/scalar differences are somewhat larger in the azimuth planes $\phi = 0°$ and $\phi = 180°$, although they are rather significant in other azimuth planes as well. As was noted above, the local underestimation is always reached at $\phi = 180°$. On the other hand, for a given μ_0 the azimuth plane of the local overestimation rotates from 0° for μ equal or close to 1 towards 90° (or, equivalently, 270°) with $\mu \to 0$ (Fig. 16). Schematically, this is illustrated in Fig. 17.

The most interesting result of our calculations is that the local overestimation reaches its maximum negative values at phase angles equal or close to 90° for all μ_0 (Fig. 15), while the local underestimation is maximum at phase angles equal or close to 0° for almost all μ_0 (Fig. 14). This remarkable result, which is invariant for all τ_0, $\tilde{\omega}$, δ, and A_L, suggests the following theoretical explanation of the large vector/scalar differences in the case of Rayleigh scattering. It is clear that,

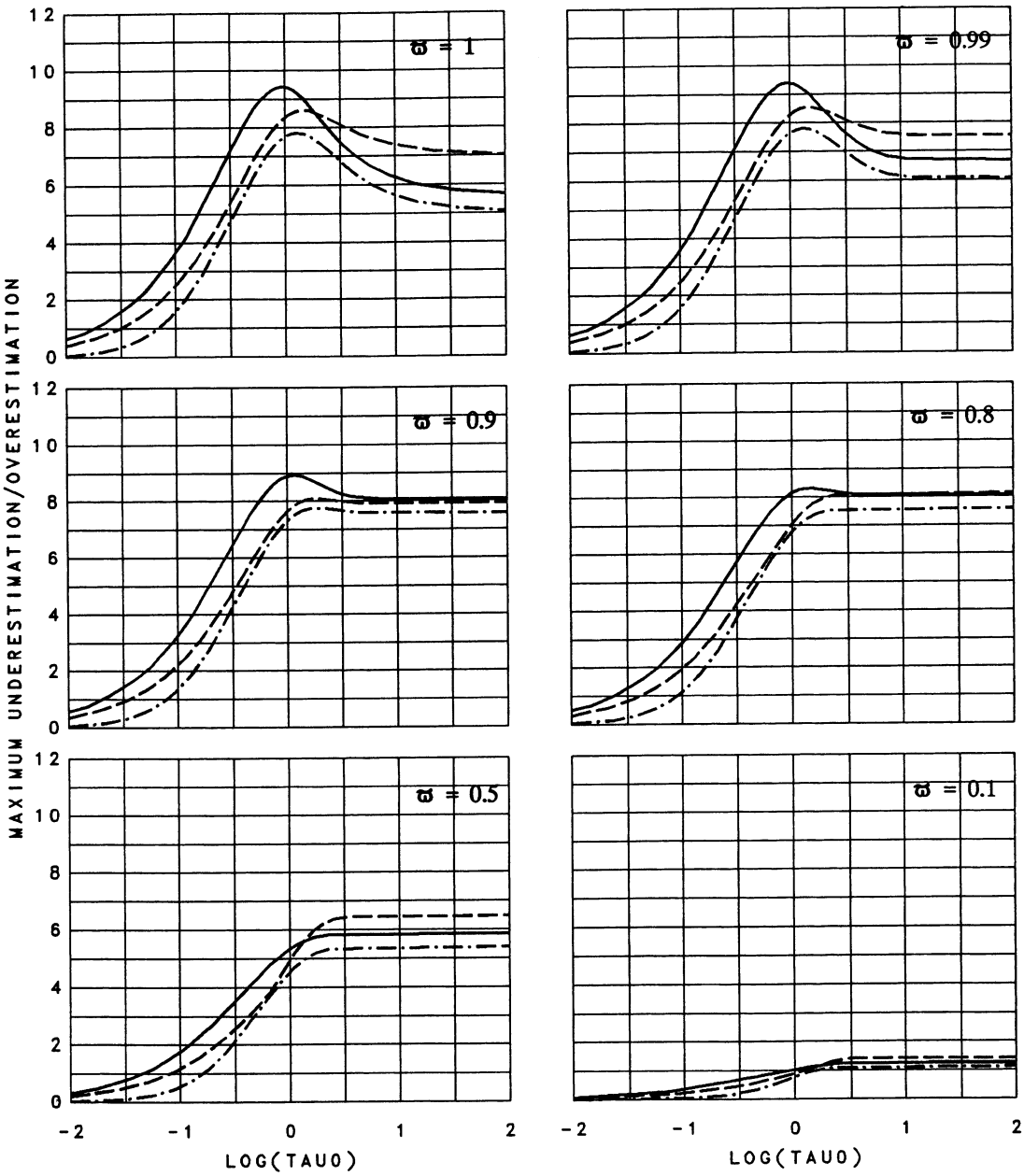

Fig. 5. Same as in Fig. 4, but for $A_L = 0.1$.

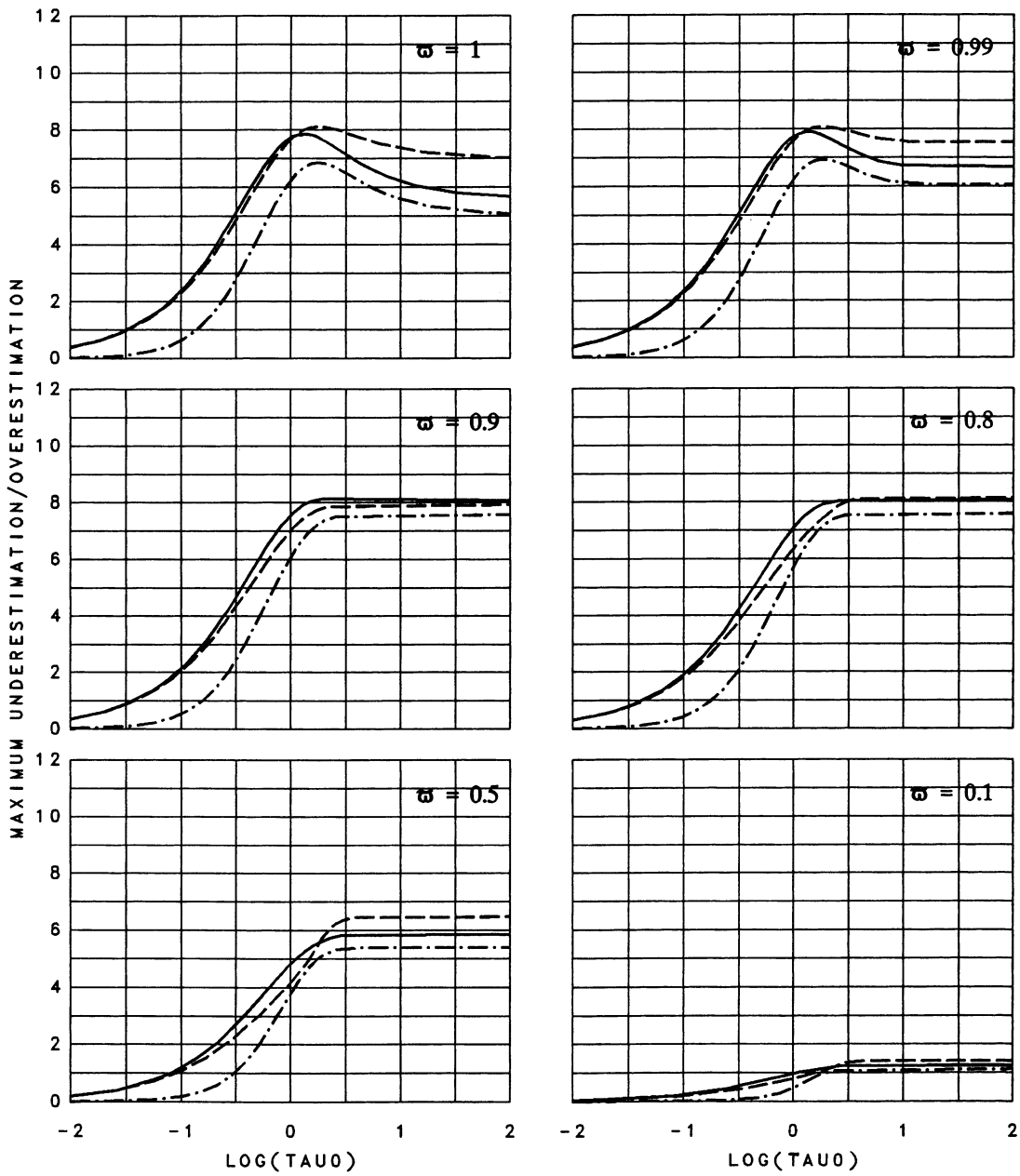

Fig. 6. Same as in Fig. 4, but for $A_L = 0.4$.

for unpolarized incident light and any directions of light incidence and reflection, the contribution of photons scattered only once to the reflected intensity is exactly the same in both vector and scalar formulations and is proportional to $P_{11}(\pi - \alpha)$, where P_{11} is the (1, 1)-element of the scattering matrix (i.e., phase function), and α is the phase angle. On the other hand, the light scattered in the atmosphere many times becomes essentially unpolarized. Therefore, it is reasonable to assume that it is photons scattered a small number of times, but more than once, which have the greatest differences between the approximate "scalar" intensity and the rigorous "vector" intensity.[1] Thus, the problem is to explain why these differences are maximum at phase angles equal or close to 0° and 90°.

In this explanation, we must take into account the following factors.

(1) Two important features of the Rayleigh scattering matrix are that Rayleigh particles are strong (perfect or almost perfect) polarizers at scattering angles near 90°, and the Rayleigh phase function is nearly isotropic.

(2) Polarization of light directly affects the intensity only through the second Stokes parameter, Q, and the element P_{12} of the scattering matrix. The effect is maximum when Q has the largest possible absolute value (i.e., when $|Q|$ is close or equal to I) and, in the case of Rayleigh scattering, when the scattering angle is close to 90° [see Eq. (6)].

(3) Unlike the intensity, the Stokes parameter Q changes not only due to light scattering, but also due to rotations of the reference plane. The maximum possible absolute change of Q due to rotations of the reference plane occurs when the angle of rotation is 90°, and Q changes its sign while not changing its absolute value [see Eq. (5)].

Thus, we can expect that low-order (and first of all second-order) light-scattering paths involving right scattering angles and right angles of rotation of the scattering plane will have the greatest vector/scalar differences. Because Rayleigh particles are nearly isotropic scatterers, the contribution

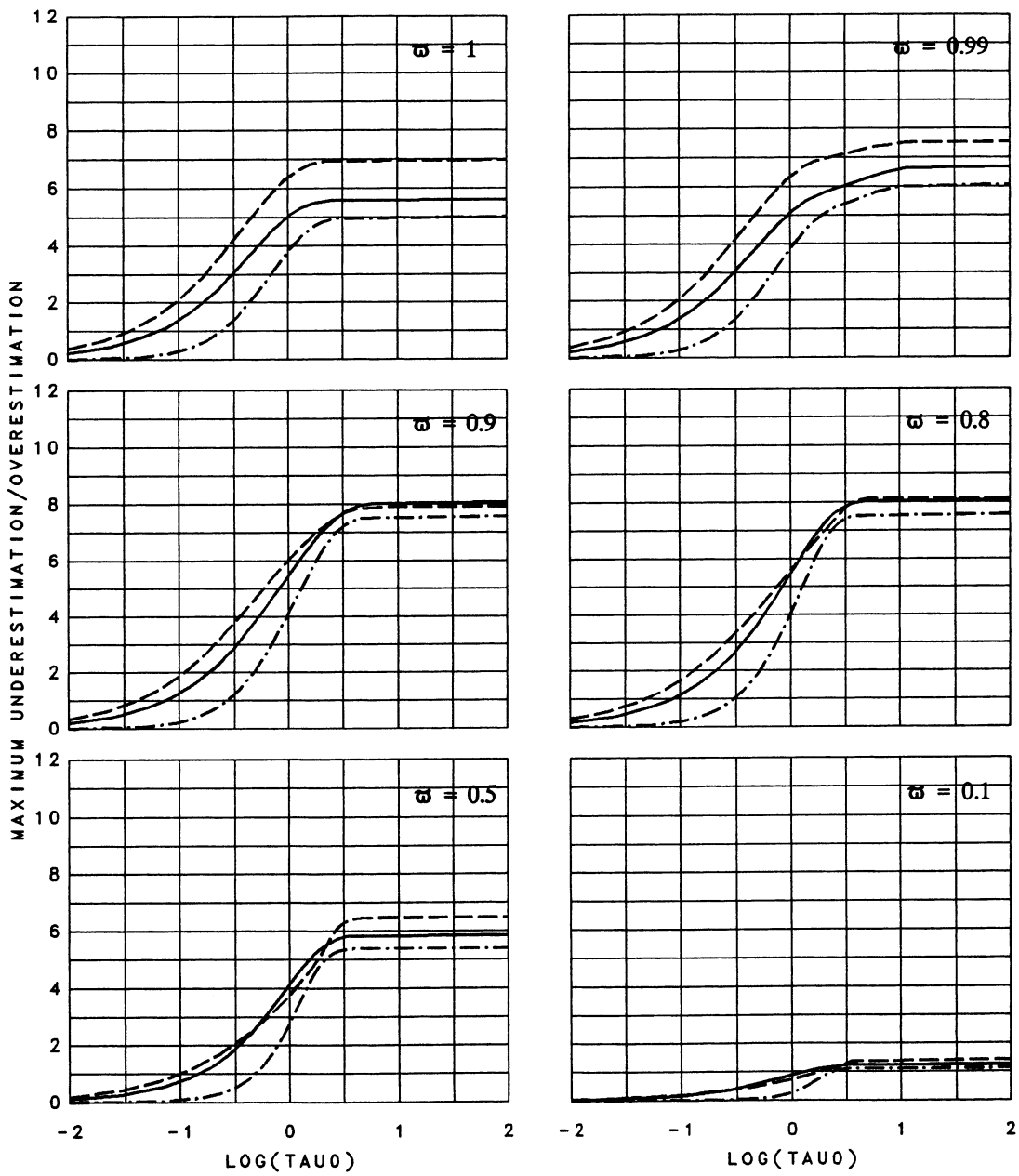

Fig. 7. Same as in Fig. 4, but for $A_L = 1.0$.

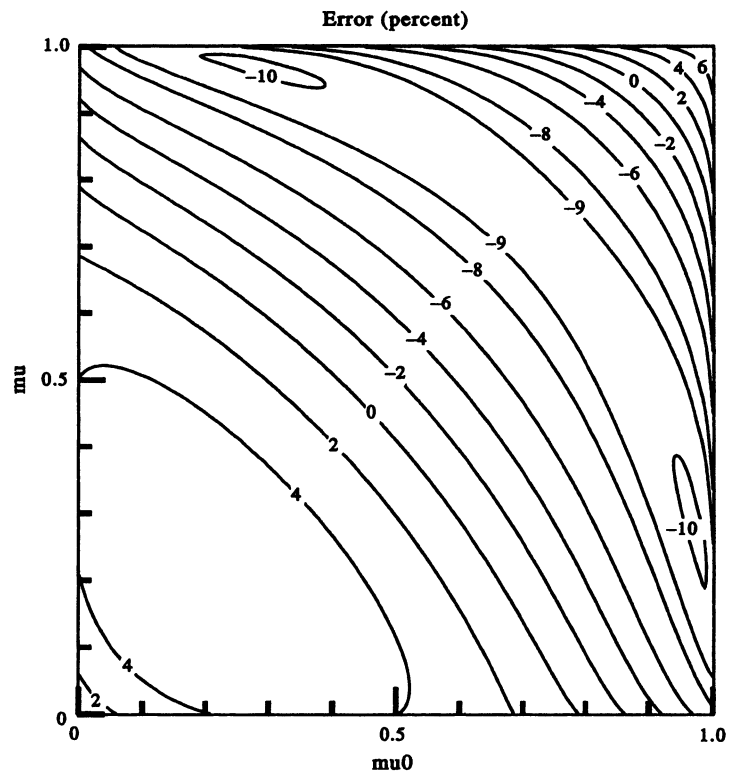

Fig. 8. Contour plot of percent error $\epsilon(\tau_0, \mu, \mu_0, \phi)$ for $\tau_0 = 1$, $\delta = 0.031$, $\tilde{\omega} = 1$, $A_L = 0$, and $\phi = 0°$.

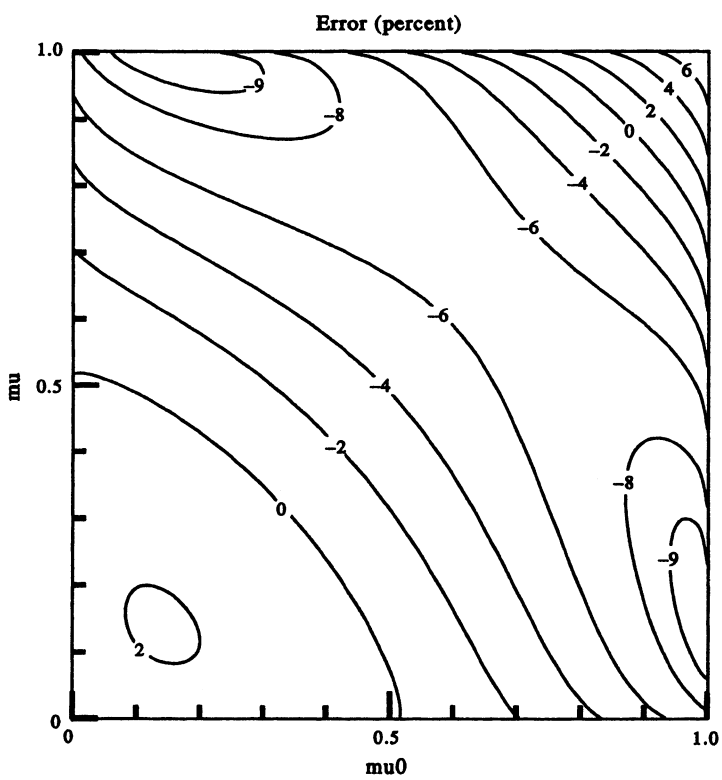

Fig. 9. Same as in Fig. 8, but for $\phi = 60°$.

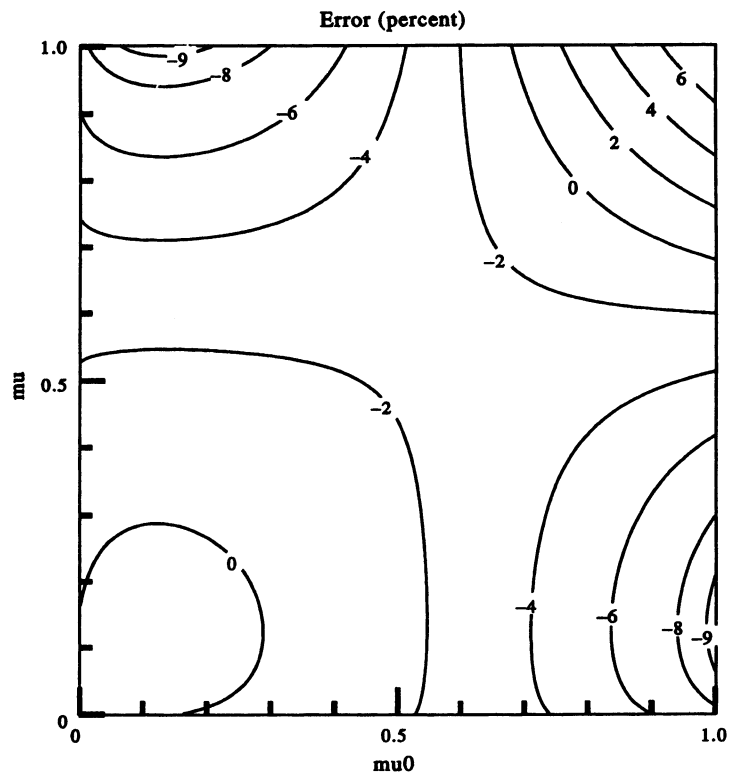

Fig. 10. Same as in Fig. 8, but for $\phi = 90°$.

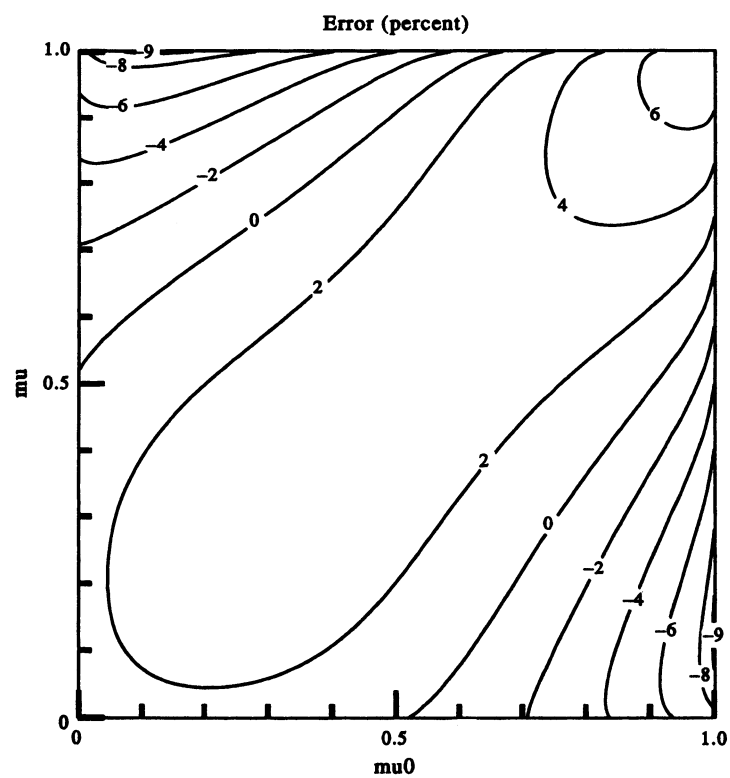

Fig. 11. Same as in Fig. 8, but for $\phi = 120°$.

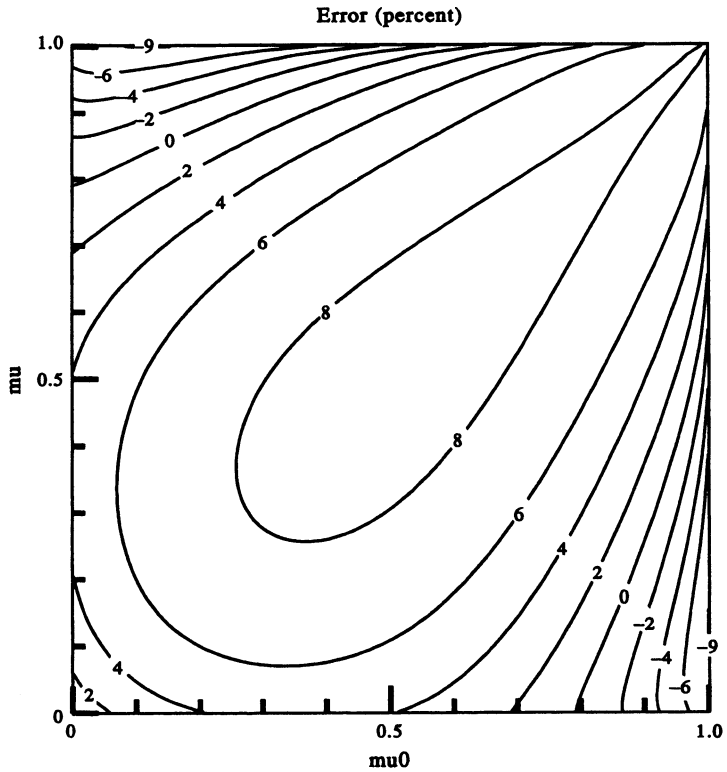

Fig. 12. Same as in Fig. 8, but for $\phi = 180°$. This diagram is also a contour plot of the local underestimation $\epsilon_u(\tau_0, \mu, \mu_0)$.

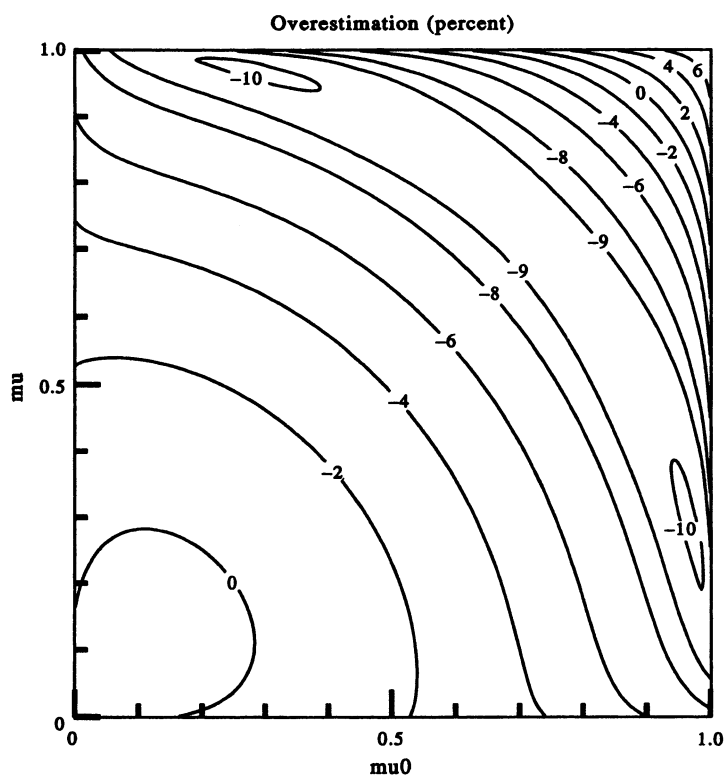

Fig. 13. Contour plot of local overestimation $\epsilon_o(\tau_0, \mu, \mu_0)$ for $\tau_0 = 1$, $\delta = 0.031$, $\tilde{\omega} = 1$, and $A_L = 0$.

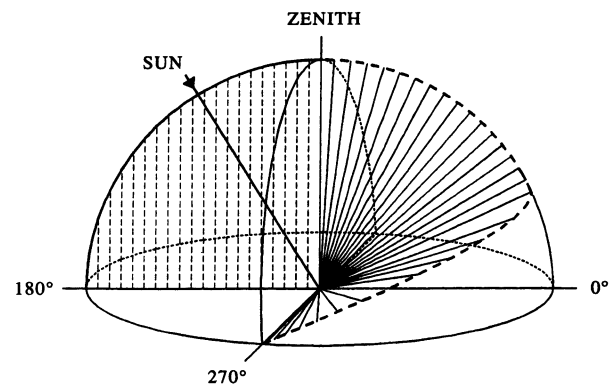

Fig. 17. Rotation of the azimuth plane at which the local overestimation is reached. The sunlight is incident in the azimuth plane $\phi_0 = 0°$. The dashed curve shows the azimuth plane of local overestimation for different directions of reflection. ϕ_u is equal to zero for μ larger than some critical value and then rotates toward 270° (or, equivalently, 90°) as μ tends to zero.

of such scattering paths to the reflected intensity will be rather significant, thus explaining large vector/scalar differences in the case of Rayleigh scattering.

Two such second-order light scattering paths are shown in Fig. 18. The left path involves two right-angle scatterings, but does not involve rotations of the scattering plane, and the resulting phase angle is equal to zero. The right path involves not only two right-angle scatterings, but also the right-angle rotation of the scattering plane, and the resulting phase angle is equal to 90°. In the scalar approximation, the contribution of these two paths to the reflected intensity is the same and, in the absence of depolarization, is proportional to $[P_{11}(90°)]^2 = 9/16$. In the rigorous vector formulation, the contribution of the left path to the reflected intensity is proportional to the (1, 1)-element of the $\bar{P}(90°)\bar{P}(90°)$ matrix which is equal to 18/16, while the contribution of the right scattering path is proportional to the (1, 1)-element of the matrix $\bar{P}(90°)\bar{L}(90°)\bar{P}(90°)$ which is equal to zero. Thus, in the first case (zero phase angle), the scalar approximation significantly underestimates the intensity, while in the second case (90° phase angle), it equally significantly overestimates the intensity, which is in full agreement with the results displayed in Figs. 14 and 15.

The relevance of this theoretical explanation is illustrated in Figs. 19–23 calculated for a semi-infinite Rayleigh atmosphere with $\tilde{\omega} = 1$ and $\delta = 0$. It is clearly seen that, in accordance with our theoretical analysis, the errors in the second-order-scattering contribution to the reflected intensity are much larger than those in the total intensity, and the errors are maximum at phase angles 0° and 90°.

4. SUMMARY AND CONCLUSIONS

The principal results of our paper are summarized in the following two points.

(1) On the basis of extensive vector and scalar multiple scattering calculations, we systematically investigated the errors induced by the neglect of polarization in calculations of the intensity of light reflected by a homogeneous, plane-parallel Rayleigh atmosphere above a Lambertian surface. We have shown that the errors decrease with increasing depolarization factor and/or increasing surface

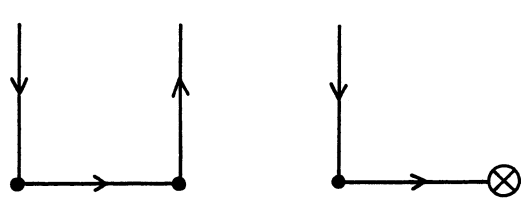

Fig. 18. Two second-order light scattering paths involving right scattering angles. The direction of propagation denoted by a crossed circle is into or out of the paper. The right path does while the left path does not involve the right-angle rotation of the scattering plane.

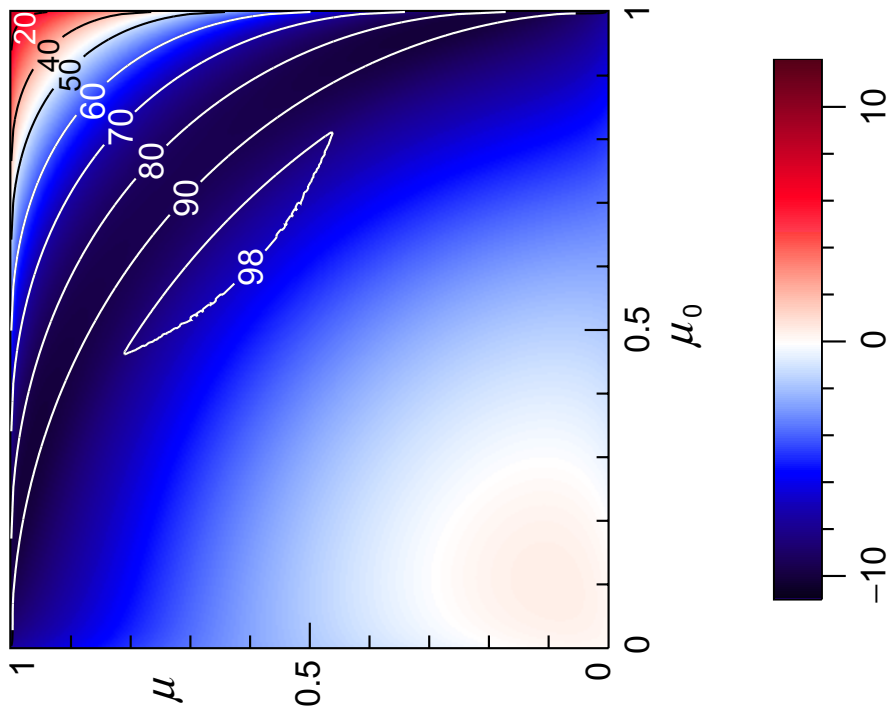

Fig. 15. Contour plot of $\alpha_o(\tau_0, \mu, \mu_0)$ versus color diagram of local overestimation $\epsilon_o(\tau_0, \mu, \mu_0)$ for $\tau_0 = 1$, $\delta = 0.031$, $\tilde{\omega} = 1$, and $A_L = 0$. Note that below and to the left of the contour labeled by 90, α_o is a continuous function of μ and μ_0, is always greater than 90°, and has a maximum at around $\mu = \mu_0 = 0.64$.

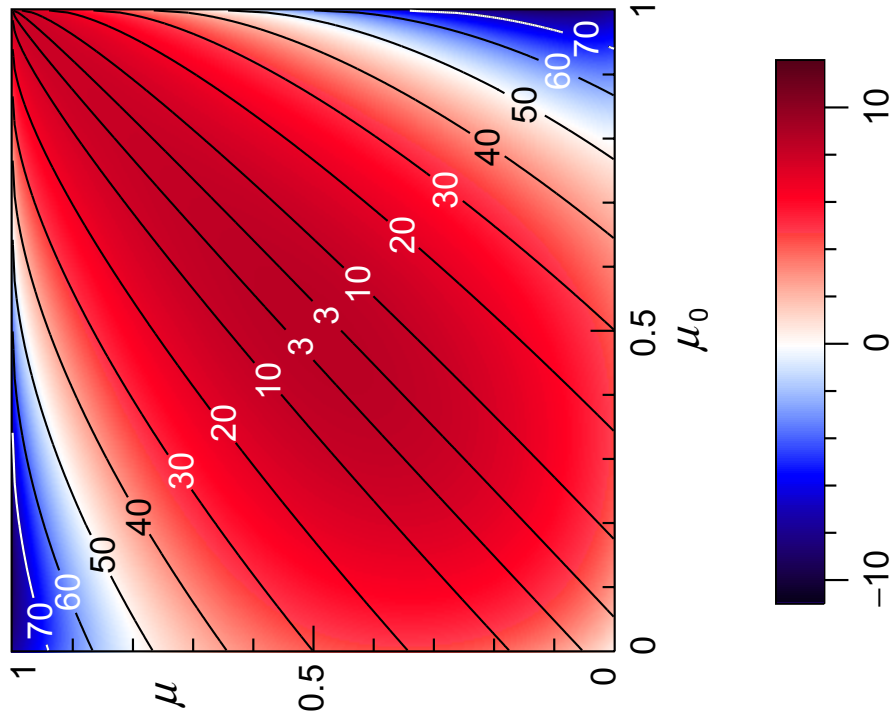

Fig. 14. Contour plot of $\alpha_u(\tau_0, \mu, \mu_0)$ versus color diagram of local underestimation $\epsilon_u(\tau_0, \mu, \mu_0)$ for $\tau_0 = 1$, $\delta = 0.031$, $\tilde{\omega} = 1$, and $A_L = 0$.

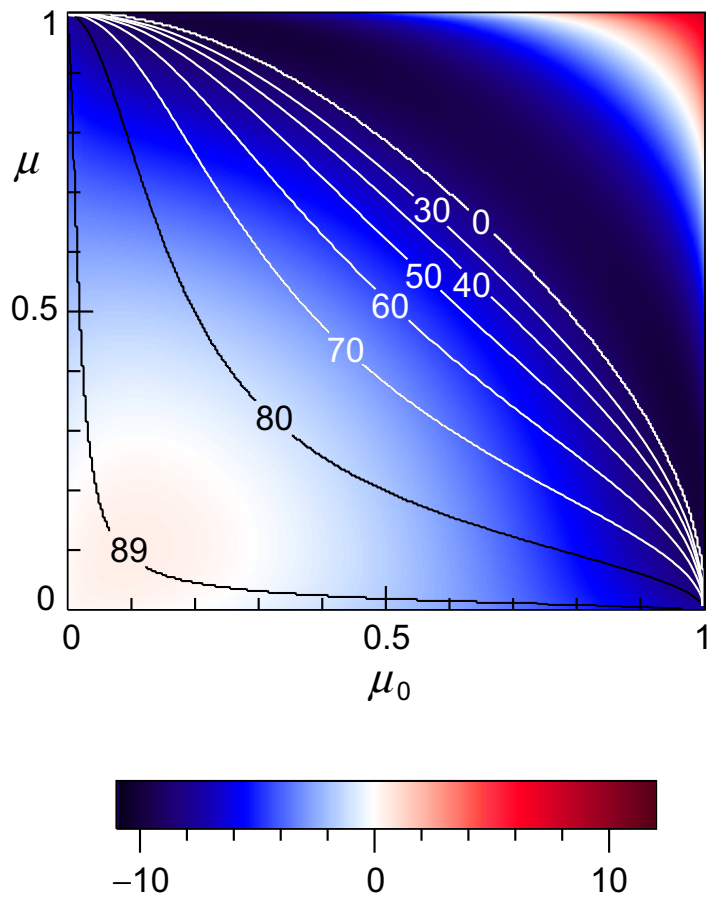

Fig. 16. Contour plot of $\phi_o(\tau_0, \mu, \mu_0)$ versus color diagram of local overestimation $\epsilon_o(\tau_0, \mu, \mu_0)$ for $\tau_0 = 1$, $\delta = 0.031$, $\tilde{\omega} = 1$, and $A_L = 0$. Note that ϕ_o is zero above and to the right of the contour labeled by 0.

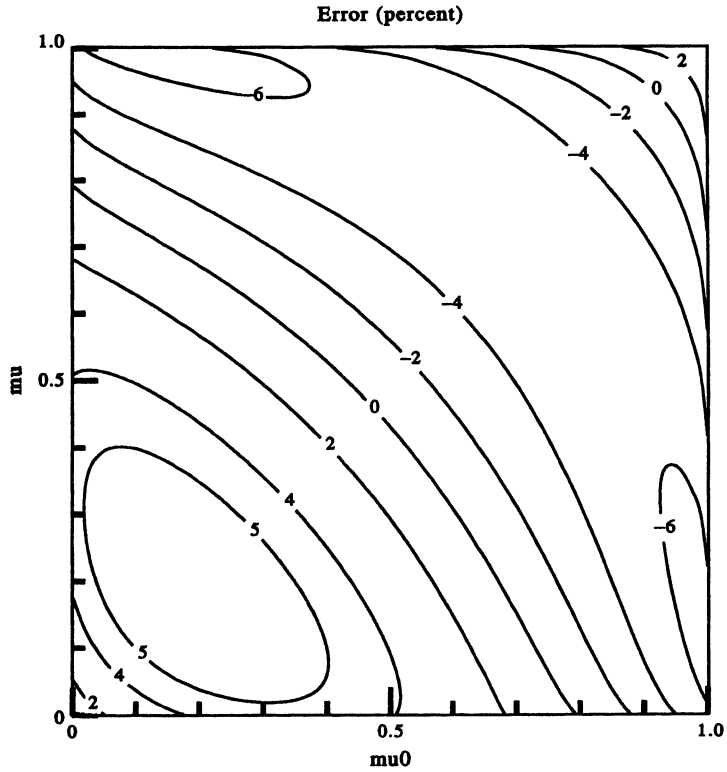

Fig. 19. Contour diagram of percent error $\epsilon(\tau_0, \mu, \mu_0, \phi)$ for $\tau_0 = \infty$, $\delta = 0$, $\tilde{\omega} = 1$, and $\phi = 0°$. Compare with Fig. 23 (lower panel, solid line) which shows the cross-section of this diagram along the 90° phase angle.

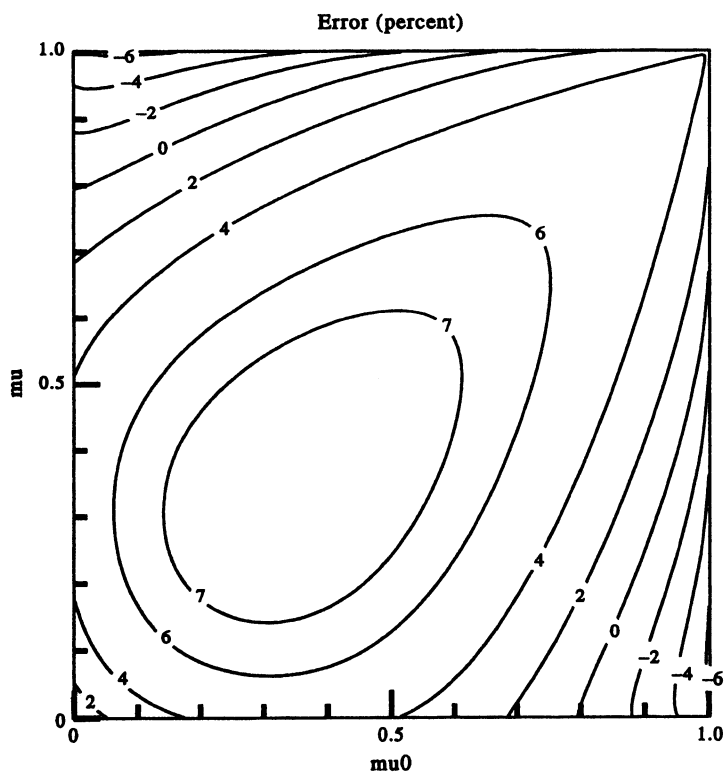

Fig. 20. Same as in Fig. 19; $\phi = 180°$. Compare with Fig. 23 (upper panel, solid line) which shows the cross-section of this diagram along the 0° phase angle.

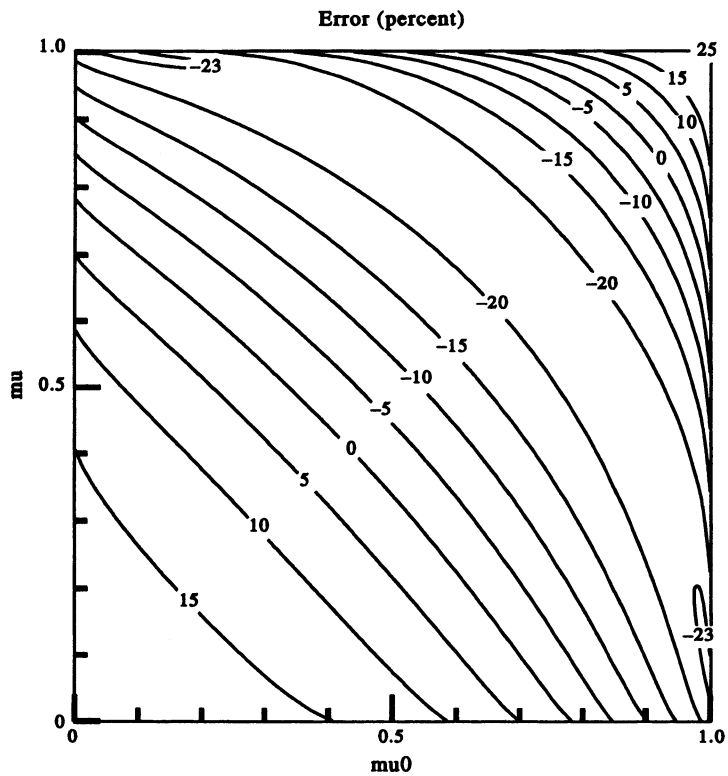

Fig. 21. Same as in Fig. 19, for the second-order-scattering contribution to the reflected intensity. Compare with Fig. 23 (lower panel, dashed line) which shows the cross-section of this diagram along the 90° phase angle.

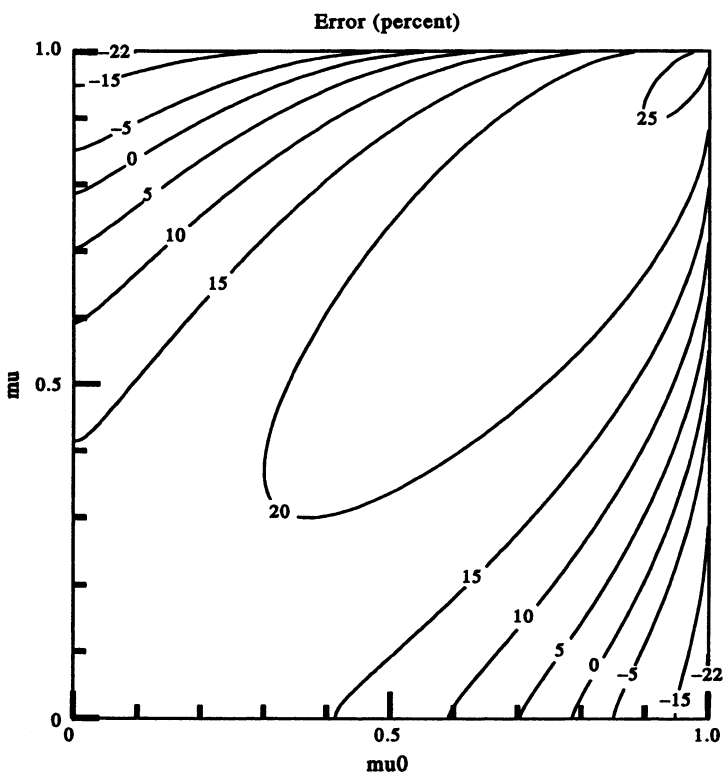

Fig. 22. Same as in Fig. 20, for the second-order-scattering contribution to the reflected intensity. Figure 23 (upper panel, dashed line) shows the cross-section of this diagram along the 0° phase angle.

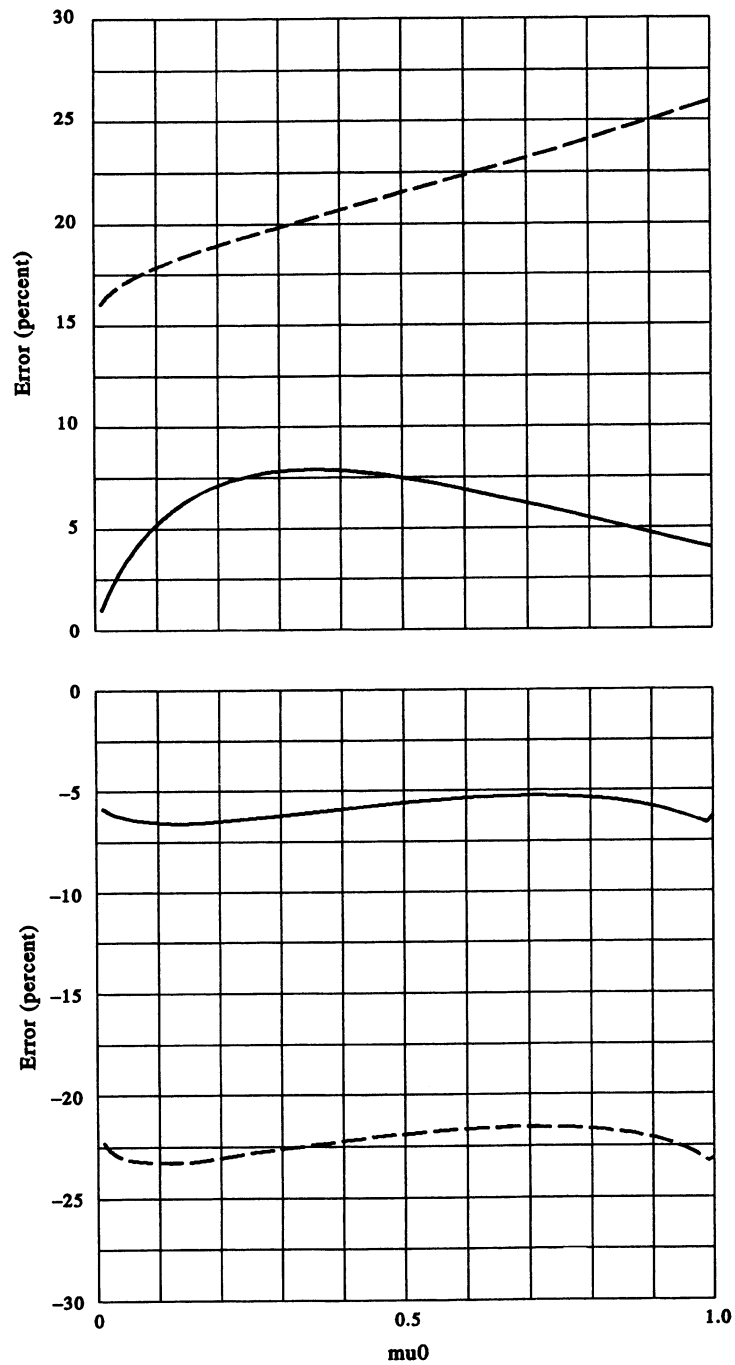

Fig. 23. Solid curves show the percent errors $\epsilon(\infty, -\mu_0, \mu_0, 180°)$ (upper panel) and $\epsilon(\infty, -[1-\mu_0^2]^{1/2}, \mu_0, 0°)$ (lower panel) for $\delta = 0$ and $\tilde{\omega} = 1$. The first of these errors corresponds to the phase angle $\alpha = 0°$, while the second one corresponds to the phase angle $\alpha = 90°$. Dashed curves show the same errors but calculated for the second-order-scattering contribution to the total reflected intensity.

albedo. For optically thin layers, vector/scalar differences always decrease with decreasing single-scattering albedo. For optically thick atmospheres, vector/scalar differences first increase as the single-scattering albedo increases from 1 to about 0.8, but then decrease with further decrease of $\tilde{\omega}$. For conservative or nearly conservative scattering (single-scattering albedo close to unity) and small surface albedos, the errors are maximum at optical thicknesses of about 1. The errors are

somewhat larger in the azimuth planes $\phi = 0°$ and $\phi = 180°$, although they are rather significant in other azimuth planes as well. Maximum errors were found at phase angles equal or close to 0° and 90°. The errors may be too large for many practical applications, and, therefore, rigorous vector calculations should be employed whenever possible. However, if approximate scalar calculations are used, we recommend to avoid geometries involving phase angles equal or close to 0° and 90°, where the errors are especially significant.

(2) We have proposed a theoretical explanation of the large vector/scalar differences in the case of Rayleigh scattering. According to this explanation, the large differences are caused by the particular structure of the Rayleigh scattering matrix (perfect or almost perfect polarization at 90° scattering angle and nearly isotropic phase function) and come from lower-order (except first-order) light scattering paths involving right scattering angles and right-angle rotations of the scattering plane. It may be noticed that similar "peculiarity" of Rayleigh scattering was also found in the problem of weak localization of light in discrete random media.[24–27]

Acknowledgements—We are grateful to B. Carlson and W. Rossow for useful discussions, J. W. Hovenier, J. Chowdhary, H. Domke, T. Viik, and an anonymous reviewer for many valuable comments and suggestions which helped us significantly improve the presentation, and J. Jonas and K. Feng for programming support. This work was supported in part by the Earth Observing System Project managed by Goddard Space Flight Center and by the Department of Energy Interagency Agreement under the Atmospheric Radiation Measurement Program.

REFERENCES

1. J. E. Hansen, *J. Atmos. Sci.* **28,** 1400 (1971).
2. S. Chandrasekhar, *Radiative Transfer*, Clarendon Press, London (1950).
3. C. N. Adams and G. W. Kattawar, *JQSRT* **10,** 341 (1970).
4. H. C. van de Hulst, *Multiple Light Scattering*, Academic Press, New York, NY (1980).
5. G. R. Bond and C. E. Siewert, *Astrophys. J.* **150,** 357 (1967); *ibid.* **164,** 97 (1971).
6. H. Domke, *Astron. Zh.* **48,** 341 (1971); *ibid.* **48,** 777 (1971).
7. W. A. de Rooij, P. B. Bosma, and J. P. C. van Hooff, *Astron. Astrophys.* **226,** 347 (1989).
8. T. Viik, *Earth, Moon, Planets* **46,** 261 (1989); *ibid.* **49,** 163 (1990); *Astrophys. Space Sci.* **178,** 133 (1991); *ibid.* **198,** 265 (1992).
9. M. J. Prather, *Astrophys. J.* **192,** 787 (1974).
10. K. H. Baines and J. T. Bergstralh, *Icarus* **65,** 406 (1986); J. B. Pollack, K. Rages, K. H. Baines, J. T. Bergstralh, D. Wenkert, and G. E. Danielson, *ibid.* **65,** 442 (1986); K. H. Baines and W. H. Smith, *ibid.* **85,** 65 (1990); K. Rages, J. B. Pollack, M. G. Tomasko, and L. R. Doose, *ibid.* **89,** 359 (1991).
11. H. R. Gordon, J. W. Brown, and R. H. Evans, *Appl. Opt.* **27,** 862 (1988); H. R. Gordon and M. Wang, *ibid.* **31,** 4247 (1992).
12. S. Mukai, *IEEE Trans. Geosci. Remote Sens.* **28,** 696 (1990).
13. G. W. Kattawar and C. N. Adams, in *Ocean Optics X*, Proc. SPIE 1302, p. 2 (1990).
14. J. Lenoble, *JQSRT* **10,** 533 (1970); E. Vermote and D. Tanré, *ibid.* **47,** 305 (1992).
15. J. E. Hansen and L. D. Travis, *Space Sci. Rev.* **16,** 527 (1974).
16. J. W. Hovenier and C. V. M. van der Mee, *Astron. Astrophys.* **128,** 1 (1983).
17. V. V. Sobolev, *Light Scattering in Planetary Atmospheres*, Pergamon Press, Oxford (1975).
18. J. W. Hovenier, *Astron. Astrophys.* **13,** 7 (1971).
19. M. Sato, K. Kawabata, and J. E. Hansen, *Astrophys. J.* **216,** 947 (1977).
20. M. I. Mishchenko, *JQSRT* **43,** 163 (1990).
21. J. M. Dlugach and E. G. Yanovitskij, *Icarus* **22,** 68 (1974).
22. W. A. de Rooij, Reflection and transmission of polarized light by planetary atmospheres, Ph.D. thesis, Free University, Amsterdam (1985).
23. J. W. Hovenier, private communication (1993).
24. M. P. van Albada and A. Lagendijk, *Phys. Rev. B* **36,** 2353 (1987).
25. M. P. van Albada, M. B. van der Mark, and A. Lagendijk, *J. Phys. D.* **21,** S28 (1988).
26. M. I. Mishchenko, *Phys. Rev. B* **44,** 12597 (1991).
27. M. I. Mishchenko, *Astrophys. J.* **411,** 351 (1993).